JMEPEG (2012) 21:418–423
DOI: 10.1007/s11665-011-9911-6

1059-9495/$19.00

The Effect of Fuel Types on Porous Alumina Produced via Soft Combustion Reaction for Implant Applications

Radin Shafinaz Jamil, Khairunisak Abdul Razak, Nurfateen Fakhariah Ahmad, and Hasmaliza Mohamad

(Submitted February 16, 2010; in revised form March 9, 2011)

This article describes the effects of fuel types on the porous structure of alumina produced using a soft combustion reaction. There are several combustion parameters that could affect the porous structure of the alumina produced such as fuel-to-oxidizer ratios, ignition temperature, and type of fuels. In this study, the effect of fuel types on alumina properties was studied. Citric acid, glycine, and urea were used as fuels along with aluminum nitrate as an oxidizer. The properties of porous alumina produced using three different fuels were compared to determine the optimum fuel that could produce the best properties for implant applications. X-ray diffraction analysis showed that single-phase alumina powder was obtained in all samples. Morphology observation using scanning electron microscope (SEM) on sintered bodies showed open pores which had potential to be used in implant applications. Porous alumina produced using glycine as fuel (AG) showed the best properties; high surface area of 8.7 m^2/g, porosity of 70% and sintered density 1.37 g/cm^3.

Keywords alumina, fuel, implant application, porous structure, soft combustion

1. Introduction

Alumina is known as an electrically insulating, optically transparent, chemically stable, bio-inert, and biocompatible material. These properties make it ideal for use in various electronic, optoelectronic, sensing, and biomedical applications. In the medical field, further research on the properties of alumina is being done for use in cell carriers, artificial organs, orthopedic, dental, and drug delivery applications (Ref 1-5). With regard to its bio-inert behavior, alumina has been structured porously for optimum function in implant applications. It has been reported that the success of the implants is dependent on the device's ability to acquire and retain stable fixation in the bony site (Ref 6). The key is to have a sphere-like and open pore structure to allow the capillaries that provide blood supply to reach the ingrown connective tissue through the pores (Ref 7). This ingrown tissue increases the interfacial area between the implant devices-tissue which further restricts the movement of the device in the implant. Therefore, biological fixation is enhanced when the interface is established by the living tissue in the pores (Ref 8).

A combustion synthesis approach is one of the wet chemical processes which have been studied to produce Cr_2O_3, Al_2O_3, ZnO powders, etc., and owing to its capability to synthesize submicron and nanoscale powders (Ref 9-11). Although there are other wet chemical processes that can yield nanocrystallines powders, they are deemed complicated as they require multi-step reaction routes and/or long processes (Ref 12). In the industry, the calcined aluminum hydroxides method is commonly used to produce high surface alumina powders. Though it is not a very complicated process, the advantage of the combustion synthesis is that high-purity powders can be obtained at a lower temperature using simpler steps, shorter synthesis time, and requires no special igniting equipment. The combustion synthesis involves exothermic reaction based on thermal decomposition of metal nitrate and fuel to produce spontaneous flame leading to foamy metal oxides as the main product, and releases non-toxic gases such as N_2, CO_2, and H_2O as by-products directly without getting oxygen from the environment (Ref 11, 13, 14). Hence, this approach is not only energy effective as it solely relies on the heat of the chemical reaction (Ref 15), but also has been claimed as an environmentally clean process (Ref 11, 16) as it releases additional products that are odorless, colorless, and not harmful. Generally, a good fuel should react non-violently, produce non-toxic gases and act as a complexant for metal cations (Ref 17) to increase the solubility and provide homogenous mixture of fuel-nitrate. Previous studies have shown that different fuels perform different thermal reactions and produce different powder morphologies (Ref 12, 18, 19). In this study, we aim to discover the fuel which can produce the optimum porous alumina structure that can potentially be used in implant applications. Fuels such as urea, glycine, and citric acid have been chosen since they are cheaper/readily available and possess good fuel characteristics. The results show that properties of alumina were dependent on the types of fuel. Glycine (AG) showed promising results for implant applications in terms of surface area, porosity, and density, compared to alumina produced using urea (AU) and citric acid (AC).

Radin Shafinaz Jamil, Khairunisak Abdul Razak, Nurfateen Fakhariah Ahmad, and **Hasmaliza Mohamad**, School of Materials & Mineral Resources Engineering, Universiti Sains Malaysia, Engineering Campus, 14300 Nibong Tebal, Penang, Malaysia. Contact e-mails: hidayah71@yahoo.com and hasmaliza@eng.usm.my.

2. Materials and Methods

Aluminum nitrate ($Al(NO_3)_3 \cdot 9H_2O$) and three types of fuels: glycine ($C_2H_5NO_2$), citric acid ($C_6H_8O_7$), and urea (CH_4N_2O)

were mixed following stoichiometry ratios in a minimum volume of deionized water to obtain transparent aqueous solutions (Table 1). The mixtures were each heated at 80 °C on a hot plate to undergo thermal dehydration to remove excess solvent. This step is important to produce viscous liquids (hereafter termed as precursors). When the viscous liquid was formed, the hot plate temperature was increased to 200 °C. At this stage, the viscous liquids swelled and auto ignited to form foamy soft-agglomerated powder.

In this study, the stoichiometry ratios were calculated according to the propellant chemistry concept whereby the stoichiometry mixtures of fuel and oxidant were theoretically correct for complete oxidation process (Ref 11). However, the x-ray diffraction analysis (XRD) revealed that the as-synthesized powder contained some impurity phases that indicated incomplete combustion process. In order to remove traces of undecomposed products, the voluminous powders were calcined in air with a ramp speed of 5 °C/min to 1100 °C, and dwelled for 2 h to obtain pure and stable phase alumina powders. The alumina powders obtained were named as AG (glycine as fuel), AU (urea as fuel), and AC (citric acid as fuel). Thermogravimetric analysis (TGA) of the powders was carried out at a heating rate of 5 °C/min in air. The phase presence in the compounds was analyzed using x-ray diffractometer using CuKα irradiation. The surface area analysis of the alumina powders was carried out using a standard BET technique with N_2 adsorption. The powders were then isostatically pressed into pellets with 150 MPa load and sintered at 1250 °C with a ramp speed of 5 °C/min. The morphology of the sintered samples was observed using scanning electron microscopy (ZUPRA VPFSEM).

3. Results and Discussion

In the soft combustion synthesis of a fuel-nitrate mixture, an exothermic reaction occurred whereby the mixture underwent a self-propagating and none explosive reaction. Different types of fuels caused different thermal reactions. Combustion reactions occurred following different fuel-to-nitrate mixtures. They can be expressed as follows (Ref 11, 13, 14):

Stoichiometry ratio of urea:aluminum nitrate

$$2Al(NO_3)_3{\cdot}9H_2O + 5CO(NH_2)_2 \rightarrow Al_2O_3 + 8N_2 + 28H_2O + 5CO_2 \quad \text{(Eq 1)}$$

$$6Al(NO_3)_3{\cdot}9H_2O + 5CO_6H_8O_7 \cdot H_2O \rightarrow 3Al_2O_3 + 9N_2 + 20H_2O + 30CO_2 \quad \text{(Eq 2)}$$

Table 1 Stoichiometry ratio and maximum temperature of the combustion reaction for different types of fuel-to-nitrate mixture

Mixture of fuel-nitrate	Stoichiometry ratio	Maximum temperature, °C
Glycine-nitrate	1.67	172
Urea-nitrate	2.5	185
Citric acid-nitrate	0.833	160

Stoichiometry ratio of glycine:aluminum nitrate

$$6Al(NO_3)_3{\cdot}9H_2O + 10C_2H_5O_2N \rightarrow 3Al_2O_3 + 14N_2 + 25H_2O + 20CO_2 \quad \text{(Eq 3)}$$

When the fuel-nitrate solutions were subjected to heat, the water in the precursor solutions evaporated and formed a sticky solution (gel). Under continuous heating, the chemicals in the gel decomposed. Decomposition of aluminum nitrate involves an elimination of nitrate groups (Ref 20) that produces oxides of nitrogen (NO_x) and yields metal oxide. The decomposition of $Al(NO_3)_3{\cdot}9H_2O$ can be expressed as below:

$$Al(NO_3)_3{\cdot}9H_2O \xrightarrow[\text{dissolvation}]{-9H_2O} Al(NO_3)_3 \rightarrow 1/2Al_2O_3 + 3/2NO_2 + 3/2NO + 3/2O_2 \quad \text{(Eq 4)}$$

The resulting NO_x result from above reaction contains oxidizing element of O_2 and this causes them to react with the reducing element from the decomposition of the fuels. When urea' and glycine's amine group decomposed, they release NH_3 in the form of gases (Ref 19), while citric acid's CH_x-containing group releases CH_3 and H_2 in the form of gases (Ref 21, 22). Redox reaction took place when both reducing and oxidizer element reacts with each other thus causing more heat and gases to generate combustion process.

The thermal behavior of as-combustion powder with different types of fuel-to-nitrate mixture was analyzed using TGA, as shown in Fig. 1. Different fuels show different thermal decomposition behaviors. Decomposition starts below 200 °C with a weight loss of 13 and 10% for AU and AC, respectively. This possibly corresponds to the loss of volatile matters as indicated by the endothermic peak on the DTA curves. For glycine, it happens at temperatures below 400 °C with a weight loss of 1.5%. Exothermic peaks do support the claim that the main decomposition occurred in the temperature range of 220-280 °C for AU. It was very steep, showing that the reaction took place rapidly. In the AC sample, the slope was less steep when compared to AU, indicating lesser decomposition at the temperature range of 200-600 °C. Meanwhile, the process occurred in the range of 400-800 °C for AG. The main decomposition occurred with weight loss of 72, 35, and 4.5% for AU, AC, and AG, respectively. This is due to the decomposition of hydroxycarbonate that might have been left over in the as-combustion powder. At temperatures above 600 °C, the decomposition of carbonate residue occurred due to low synthesis temperature (below 200 °C) that caused an incomplete combustion reaction (Fig. 2).

3.1 X-ray Diffraction Analysis

Figure 3(a) shows an XRD spectra of as-combusted powders. AC and AG were in amorphous structure. Although AU was in crystalline structure, the presence of phases, δ-Al_2O_3 and θ-Al_2O_3, in the samples shows that the transaction of alumina phases is yet to reach alpha phases. At about 820 °C, an intense peak was observed for AC samples. According to Chandradass et al. (Ref 18), the intense exothermic peak corresponds to the powder crystallization. To explain the structural changes, XRD was carried out for powders calcined at 800 °C. The XRD spectra (Fig. 3b) shows structural change from amorphous to semi-crystalline, indicating the presence of δ-Al_2O_3 and γ-Al_2O_3 phases. The exothermic process

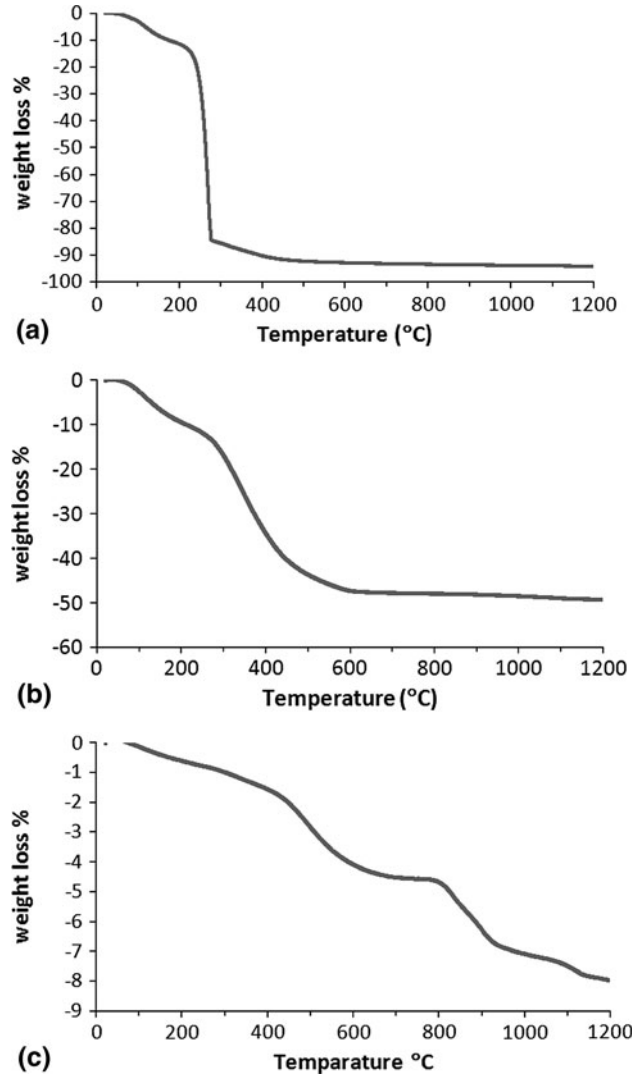

Fig. 1 TGA curves of alumina powders synthesized using different types of fuel; (a) urea, (b) citric acid, and (c) glycine

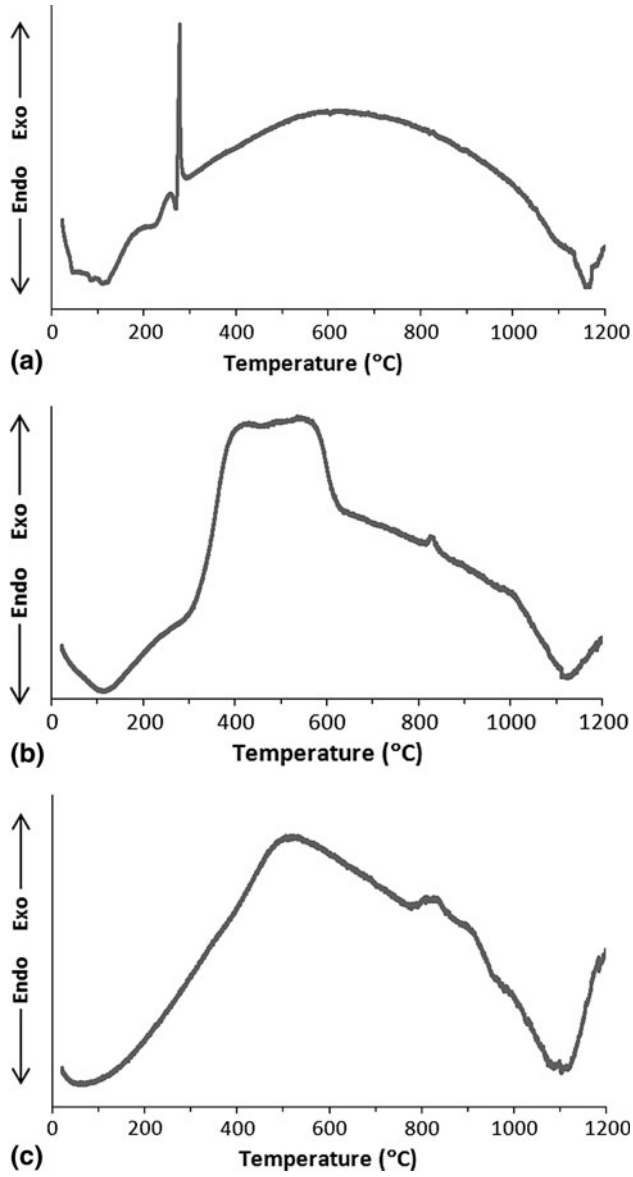

Fig. 2 DTA curves of alumina powders synthesized using different types of fuel; (a) urea, (b) citric acid, and (c) glycine

concluded above 1100 °C. When powders were subjected to calcination at that temperature, well crystalline peaks corresponding to α-Al_2O_3 phases were observed. Therefore, the calcination temperature was chosen to be at 1100 °C to obtain pure α-Al_2O_3 phases (Fig. 3c).

The crystallite size was calculated from XRD analysis using Scherrer's formula taken at (300) peak of calcined powders x-ray pattern as shown in Table 2 (Ref 23).

$$D = 0.9\lambda/\beta\cos\theta \quad \text{(Eq 5)}$$

where D is the crystallite size in nm, λ is the radiation wavelength (0.1542 nm), θ is the diffraction peak angle, and β is the line width at half peak intensity. β can be calculated using the Gaussian function:

$$\beta^2 = \beta_m^2 - \beta_s^2 \quad \text{(Eq 6)}$$

where β_m is the measured full width at half maxima (FWHM) and β_s is the FWHM of a standard silicon sample.

The use of citric acid as fuel creates AC with larger crystallite size as compared to AU and AG. The lowest maximum temperature was generated and it helps to ensure that the agglomerate did not break during the calcination process. When the agglomerate slowly increases its size with the lowest maximum temperature this creates crystallite size with larger size (Ref 14). The surface area of AC was the lowest when compared to AU and AG, and this correlated with the density results of alumina powders calcined at 1100 °C (see Table 2) which were obtained by pycnometer measurement. AU has the highest surface area when compared to AC and AG. The surface area result was in good agreement with the SEM micrographs whereby the microstructure of porous AU consisted of more pores compared to AG and AC (Fig. 4; Table 3).

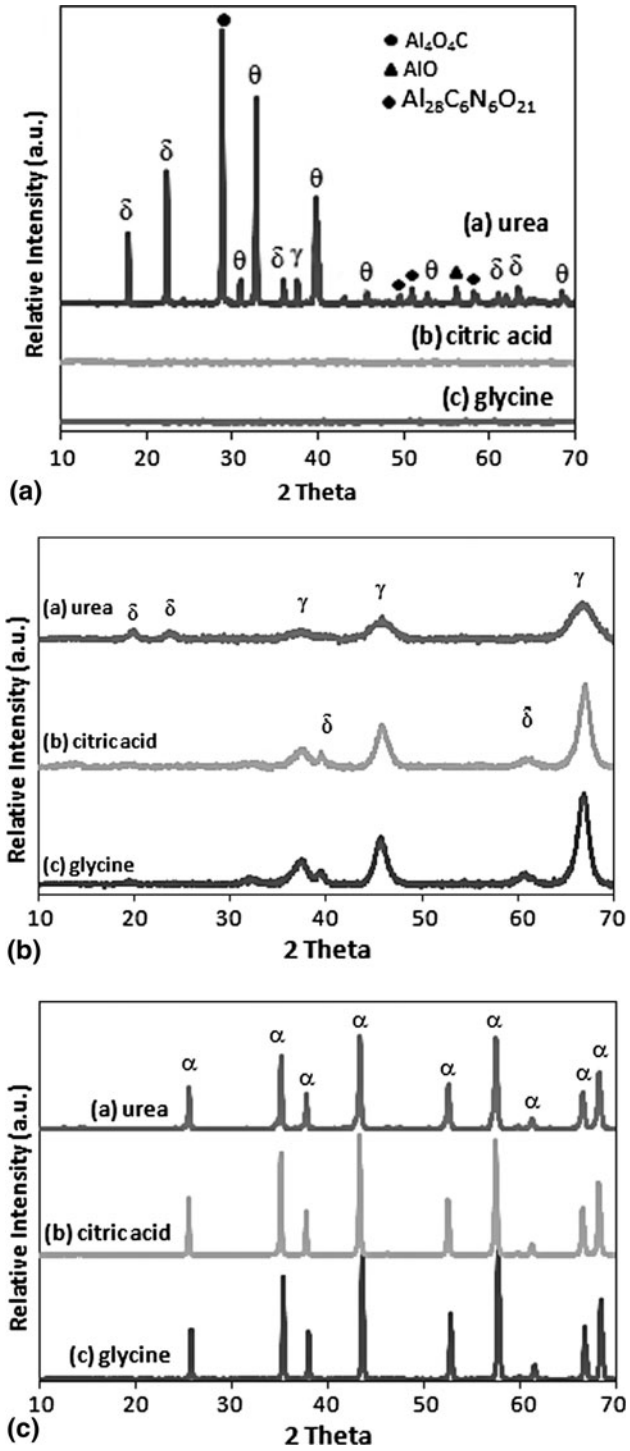

Fig. 3 XRD spectra of synthesized porous alumina prepared by three types of fuels: (a) as-synthesized powder, (b) samples calcined at 800 °C, and (c) samples calcined at 1100 °C

3.2 Microstructure Analysis

Microstructure analysis showed that different types of fuels resulted in different microstructures of porous alumina powders as shown in Fig. 4 and 5. The AG sample possessed a sphere-like and open pore structure, while the AC sample consisted of spherical pores with closed pores that were not well distributed (Fig. 4). On the other hand, AU had a coral-like structure with the existence of interconnected pores. In this study, pore size was measured from SEM micrographs. AG had the largest pore size with a size range of up to submicron scale (50-630 nm). This result proved that a higher surface area can be obtained using AG. The pattern observed in glycine samples is concurrent with previous study (Ref 12) where they acquire more loose and porous structure that can be attributed to the evolution of large amount of gases during combustion reaction. Even though AU has the highest temperature during the combustion process, the characteristic of its indecent flame growing after auto-ignition may cause partial sintering resulting in pore size shrink. For AU and AC, pore sizes were in the range of 10-90 nm and 20-90 nm, respectively.

In this study, porous alumina produced was aimed toward implant applications. To fit the material to this application, alumina powder was pressed into a body and sintered at 1250 °C. The fractured surface micrographs of the body are illustrated in Fig. 5. The microstructures for all samples were porous but for different types of fuels, the pore structures and pore sizes were also different. For AC and AG samples (Fig. 5b and c), foamy agglomerated structures were obtained. All samples showed larger pore sizes after the sintering process. The pore size of AU increased to 40-80 nm, AC to 150-210 nm and AG to 130-220 nm. The increase of pore size of the sintered body is possibly due to the uneven pore size of the powders. The pressing process does not fragment the pore size to be uniform and lead to a slower and non-uniform densification during the sintering process. The agglomerated structure of a compacted powder also contributes to larger pores. Agglomerates do looser packing. When compacted powder densifies, free surfaces are replaced by grain boundaries that migrate leading to grain growth. However, the densification occurs unevenly and causes some parts to become rigid, preventing optimum densification between agglomerations and creating large pores around the locally densifying particle agglomerates. In this study, the combustion method using urea, glycine, and citric acid as fuel produced porous structures with a

Table 2 Specific surface area and crystallite size of alumina powders produced by using urea (AU), citric acid (AC), and glycine (AG)

Sample	Density, g/cm^3	Specific surface area, cm^2/g	Crystallite size, nm
AU	2.94	9.00	26.8
AC	3.01	1.85	31.9
AG	2.98	7.18	29.8

Table 3 Density and surface area of compacted alumina sintered at 1250 °C

Samples	Density, g/cm^3	Surface area, m^2/g	Apparent Porosity, %
AU	2.2	6.6	60
AC	3.4	5.2	35
AG	1.4	8.7	70

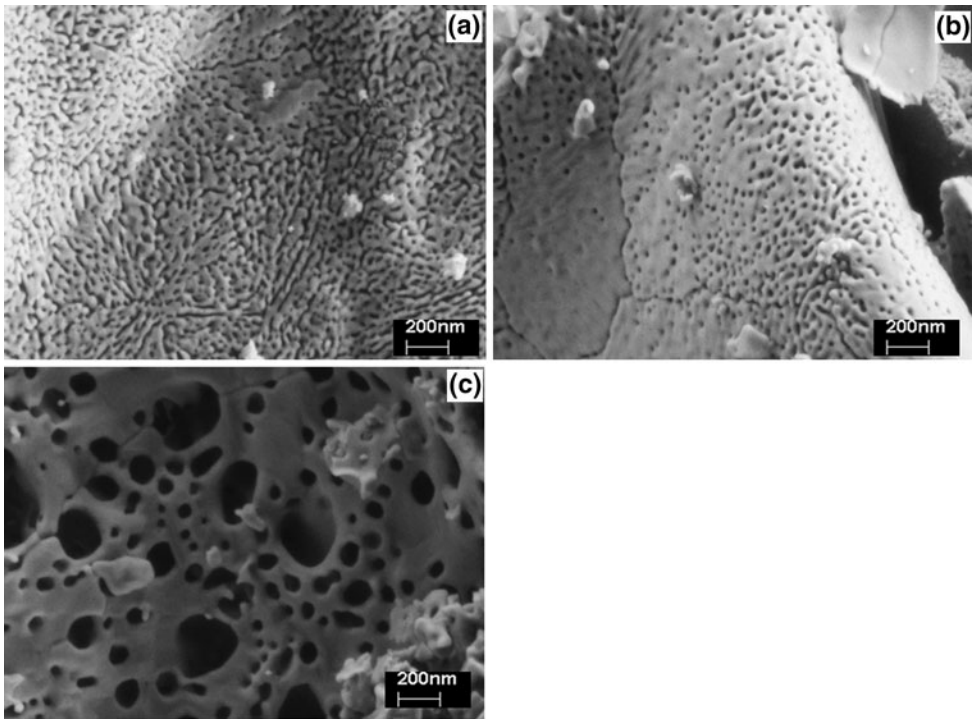

Fig. 4 SEM micrographs of porous alumina produced by using different fuels (a) AU, (b) AC, and (c) AG

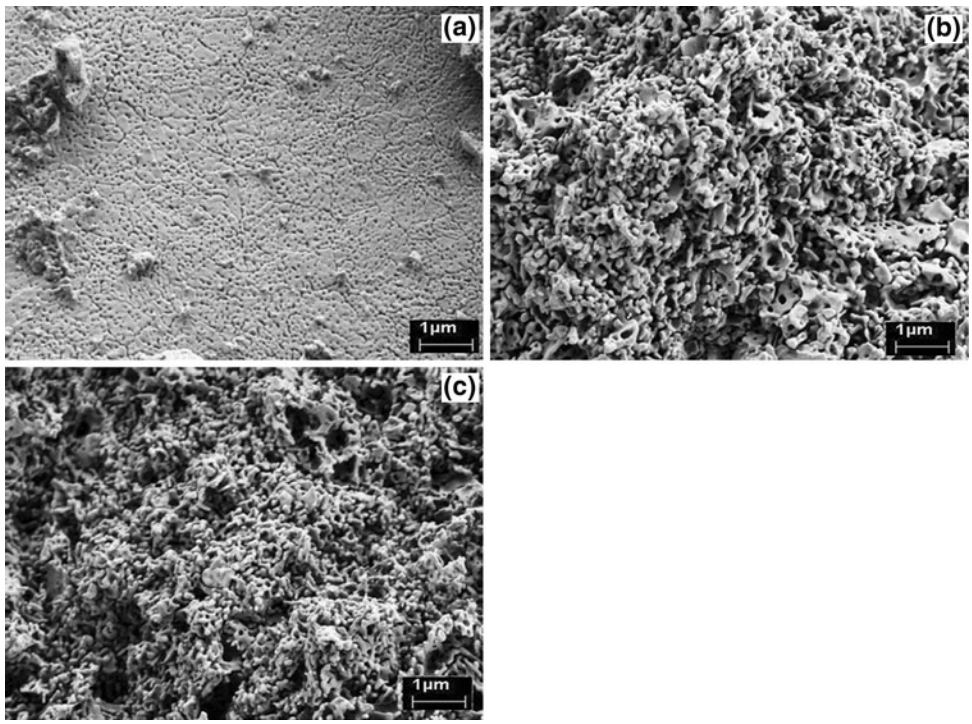

Fig. 5 SEM micrographs of fractured surface of porous alumina produced using different types of fuels (a) AU, (b) AC, and (c) AG. The samples were sintered at 1250 °C

presence of open pores that are likely to meet requirements for implant applications. For AU, the porous structure is most likely to have intergranular pore shapes although in compacted form, while AG and AC have spherical-like porous structure.

4. Conclusion

In this study, porous alumina powders were successfully produced by soft combustion technique using different types of

fuel, i.e., glycine (AG), urea (AU), and citric acid (AC). Pure α-Al_2O_3 phase was obtained after calcination at 1100 °C. AG possessed the largest surface area, lowest density, and the optimum pore size that could be beneficial for implant applications, compared to AC and AU.

Acknowledgments

The authors acknowledge the technical support from School of Materials and Mineral Resources Engineering, Universiti Sains Malaysia. This research was funded by USM Short Term Grant 6035292.

References

1. K.L. Eckert, M. Mathey, J. Mayer, F.R. Homberger, P.E. Thomann, P. Groscurth, and E. Wintermantel, Preparation and In Vivo Testing of Porous Alumina Ceramics for Cell Carrier Applications, *Biomaterials*, 2000, **21**(1), p 63–69
2. D.F. Williams, *Materials Science and Technology*, Vol 14, VCH, New York, 1992
3. S. Aleksandar and M. Rakin, Biomaterials—Joints and Problems of Contact Interfaces, *FME Trans.*, 2006, **34**(2), p 81–86
4. J. Chevalier, P. Taddei, L. Gremillard, S. Deville, G. Fantozzi, J.F. Bartolomé, C. Pecharroman, J.S. Moya, L.A. Diaz, R. Torrecillas, and S. Affatato, S., Reliability Assessment in Advanced Nanocomposite Materials for Orthopaedic Applications, *J. Mech. Behav. Biomed. Mater.*, in press, corrected proof, 2010
5. E. Gultepe, D. Nagesha, S. Sridhar, and M. Amiji, Nanoporous Inorganic Membranes or Coatings for Sustained Drug Delivery in Implantable Devices, *Adv. Drug Deliv. Rev.*, 2010, **62**, p 305–315
6. K.C. Popat, E.E. Leary Swan, V. Mukhatyar, K.-I. Chatvanichkul, G.K. Mor, C.A. Grimes, and T.A. Desai, Influence of Nanoporous Alumina Membranes on Long-Term Osteoblast Response, *Biomaterials*, 2005, **26**(22), p 4516–4522
7. G. Selvaduray, *Ceramics as Biomaterials, Lecture Note for Biomaterials and Biomedical Devices (MatE 175)*, St Jose State University, St Jose, California, 2005
8. B.D. Ratner, A.S. Hoffman, F.J. Schoen, and J.E. Lemons, *Biomaterials Science: An Introduction to Materials in Medicine*, Academic Press, Millbrae, CA, 1996
9. C.-C. Hwang and T.-Y. Wu, Synthesis and Characterization of Nanocrystalline ZnO Powders by a Novel Combustion Synthesis Method, *Mater. Sci. Eng. B*, 2004, **111**(2–3), p 197–206
10. M.D. Lima, R. Bonadimann, M.J. de Andrade, J.C. Toniolo, and C.P. Bergmann, Nanocrystalline Cr_2O_3 and Amorphous CrO_3 Produced by Solution Combustion Synthesis, *J. Eur. Ceram. Soc.*, 2006, **26**(7), p 1213–1220
11. J.C. Toniolo, M.D. Lima, A.S. Takimi, and C.P. Bergmann, Synthesis of Alumina Powders by the Glycine-Nitrate Combustion Process, *Mater. Res. Bull.*, 2005, **40**(3), p 561–571
12. C.A. da Silva, N.F.P. Ribeiro, and M.M.V.M. Souza, Effect of the Fuel Type on the Synthesis of Yttria Stabilized Zirconia by Combustion Method, *Ceram. Int.*, 2009, **35**(8), p 3441–3446
13. J. Li, Y. Wu, Y. Pan, and J. Guo, Alumina Precursors Produced by Gel Combustion, *Ceram. Int.*, 2007, **33**(3), p 361–363
14. K. Tahmasebi and M.H. Paydar, The Effect of Starch Addition on Solution Combustion Synthesis of Al_2O_3-ZrO_2 Nanocomposite Powder Using Urea as Fuel, *Mater. Chem. Phys.*, 2008, **109**(1), p 156–163
15. A. Varma and A. Mukasyan, Combustion Synthesis of Advanced Materials: Fundamentals and Applications, *Korean J. Chem. Eng.*, 2004, **21**, p 527
16. J. McKittrick, L.E. Shea, C.F. Bacalski, and E.J. Bosze, The Influence of Processing Parameters on Luminescent Oxides Produced by Combustion Synthesis, *Displays*, 1999, **19**(4), p 169–172
17. J. Kishan, V. Mangam, B.S.B. Reddy, S. Das, and K. Das, Aqueous Combustion Synthesis and Characterization of Zirconia-Alumina Nanocomposites, *J. Alloys Compd.*, 2010, **490**(1–2), p 631–636
18. J. Chandradass, M. Balasubramanian, D-s Bae, and K.H. Kim, Effect of Different Fuels on the Alumina-Ceria Composite Powders Synthesized by Sol-Gel Auto Combustion Method, *J. Alloys Compd.*, 2009, **479**(1–2), p 363–367
19. C.-C. Hwang, T.-Y. Wu, J. Wan, and J.-S. Tsai, Development of a Novel Combustion Synthesis Method for Synthesizing of Ceramic Oxide Powders, *Mater. Sci. Eng. B*, 2004, **111**(1), p 49–56
20. B. Pacewska and M. Keshr, Thermal Transformations of Aluminium Nitrate Hydrate, *Thermochim. Acta*, 2002, **385**(1–2), p 73–80
21. J. Chandradass, M.H. Kim, and D.-S. Bae, Influence of Citric Acid to Aluminium Nitrate Molar Ratio on the Combustion Synthesis of Alumina-Zirconia Nanopowders, *J. Alloys Compd.*, 2009, **470**(1–2), p L9–L12
22. J. Yuwen, Y. Shaoguang, H. Zhenghe, and H. Hongbo, Sol-Gel Autocombustion Synthesis of Metals and Metal Alloys, *Angew. Chem.*, 2009, **121**(45), p 8681–8683
23. R.D. Purohit, B.P. Sharma, K.T. Pillai, and A.K. Tyagi, Ultrafine Ceria Powders Via Glycine-Nitrate Combustion, *Mater. Res. Bull.*, 2001, **36**(15), p 2711–2721